ISSN 0021-3640, JETP Letters, 2020, Vol. 111, No. 8, pp. 456–462. © Pleiades Publishing, Inc., 2020.

CONDENSED MATTER

Tuning of the Electronic and Vibrational Properties of Transition Metal Selenides TSe_2 (T = Os, Ru) and Their Metallization at High Pressures

P. G. Naumov[a, b], A. O. Baskakov[b, *], S. S. Starchikov[b], I. S. Lyubutin[b], Yu. L. Ogarkova[b], M. V. Lyubutina[b], O. I. Barkalov[c], and S. A. Medvedev[a]

[a] *Max Planck Institute for Chemical Physics of Solids, Dresden, 01187 Germany*

[b] *Shubnikov Institute of Crystallography, Federal Scientific Research Centre Crystallography and Photonics, Russian Academy of Sciences, Moscow, 119333 Russia*

[c] *Institute of Solid State Physics, Russian Academy of Sciences, Chernogolovka, Moscow region, 142432 Russia*

**e-mail: arseniybaskakov@gmail.com*

Received March 27, 2020; revised March 27, 2020; accepted March 29, 2020

We present a systematic analysis of electrical properties of two transition metal selenides $OsSe_2$ and $RuSe_2$ under conditions of low temperature down to 1.8 K and external pressure up to 43 GPa. Both compounds have a pyrite-type crystal structure under ambient conditions and, according to Raman spectroscopy, do not undergo phase transitions up to the highest pressures. $OsSe_2$ and $RuSe_2$ undergo semiconductor-to-metal transitions at pressures up to 15 GPa. Further increase in pressure leads to the appearance of a superconducting transition at low temperatures. At 40 GPa, the critical temperatures of the superconducting transition reach maximum values of 5.5 and 6 K for $RuSe_2$ and $OsSe_2$, respectively.

DOI: 10.1134/S0021364020080044

INTRODUCTION

In recent decades, considerable interest has been focused on the structural, electronic, optical, and chemical properties of transition metal dichalcogenides (TMDs) TX_2 (T is a transition metal cation and X is a chalcogen anion) [1–6]. The weak van der Waals bonding [1] between the two-dimensional TMDs atomic layers allows the formation of various low-dimensional structures that can compete with graphene in important technical applications, including nanoelectronics, photonics and energy storage [7, 8]. In this case, TMDs exhibit a significant variety of electronic properties [1]. As for the type of conductivity, TMDs can be both insulators and semiconductors, as well as metals and superconductors [7]. Moreover, their electronic and structural properties can be significantly modified by chemical substitution and the application of high pressure [9–12]. Thus, in $PdSe_2$ and PdS_2, which have an orthorhombic structure of the PdS_2 type (*Pbca* space group), external pressure induces a structural transition to a pyrite-type structure ($Pa\bar{3}$ space group). This transition is accompanied by metallization and a transition to the superconducting state at low temperatures [13, 14]. The critical temperature of the superconducting transition T_c reaches 13.1 K in $PdSe_2$ at 23.0 GPa [13], and 8.0 K in PdS_2 at 37.4 GPa [14]. Raman spectroscopy established a direct correlation between the T_c value and the strength of Se–Se bonds in palladium diselenide.

Another example of a chalcogenide with a pyrite structure exhibiting superconducting properties is $IrSe_2$–$RhSe_2$ solid solution, which was studied at the Tokyo Institute of Technology [15]. It turned out that the highest T_c value is achieved in the chemical composition $Ir_{0.58}Rh_{0.36}Se_2$. This is associated with destabilization of the Se–Se bonds and partial transfer of electrons from Ir and Rh to Se.

$OsSe_2$ is a diamagnetic semi-metal with a pyrite-type structure [16, 17]. Using ab initio calculations, it was shown that osmium diselenide can have symmetry protected energy and direction-dependent spin surface textures on the (001) surface [18]. $RuSe_2$ is a diamagnetic semiconductor with an indirect band gap at ambient pressure [19, 20]. The quantum dots of $RuSe_2$, nanotubes and nanoparticles have recently been synthesized, which are promising materials for nanotechnology applications [21–23]. $RuSe_2$ also exhibited the thermoelectric behavior with a Seebeck coefficient of –200 μV/K near 730 K [20]. However, the structural and electronic transport properties of $RuSe_2$ have not yet been studied under high pressure.

In previous works on $PdSe_2$ and $Ir_{0.94-x}Rh_xSe_2$, the presence of a correlation between the Se–Se oscillation frequency and the critical temperature of the superconducting transition was shown. Some correlations can also be expected between the pyrite-type structure of TMDs and the appearance of a superconducting state. In this direction, it is interesting to study and compare the transport properties and phonon modes of osmium diselenide $OsSe_2$ and ruthenium diselenide $RuSe_2$ under high-pressure conditions.

EXPERIMENT

$OsSe_2$ and $RuSe_2$ single-crystal samples were synthesized by the chemical vapor transport method using polycrystalline $OsSe_2$ and $RuSe_2$ as starting materials. First, polycrystalline compounds of $OsSe_2$ and $RuSe_2$ were synthesized by a direct reaction of the elemental Os (Alfa Aesar 99.95%) or Ru (Alfa Aesar 99.95%), respectively, with Se (Alfa Aesar 99.999%) at 800°C in an evacuated fused silica tube during over 10 days. The phase purity of the obtained microcrystalline powder was confirmed by X-ray powder diffraction. Starting synthesis with microcrystalline powder, the single crystals of $OsSe_2$ and $RuSe_2$ were grown by a chemical transport reaction using the temperature gradient method (with 600°C for the source and 500°C for the sink) with $PdCl_2$ (Alfa Aesar 99.9%) as a transport additive. The stoichiometry of the obtained crystals was proved using energy dispersive X-ray spectroscopy. A screw-clamped diamond anvil cell equipped with 550 μm culet diamond anvils was used for the simultaneous Raman spectroscopy and electrical resistivity measurements. The gasket was made of a 300 μm thick tungsten foil. To measure the electrical resistivity, the tungsten gasket was insulated with a cubic BN/epoxy mixture. Almost square-shaped single-crystal samples with a characteristic size of about 190 μm in the plane and a thickness of about 5–10 μm were loaded into the sample chamber (diameter 200 μm and height 40 μm) filled with NaCl as a pressure-transmitting medium. Four electrical leads fabricated from Pt foil 5 μm thick were attached firmly to the sample surface by applying pressure to the anvils. The dc resistivity of the sample was measured in the van der Pauw configuration (see Fig. 1) in the temperature range from 1.8 K to room temperature. Raman spectra were collected at room temperature in the backscattering geometry using a customary confocal micro-Raman spectrometer equipped with a 20X long working distance objective. A He–Ne laser as an excitation source with a wavelength of 632.8 nm and a single-grating spectrograph with a resolution of 1 cm^{-1} were used in the experiment. Pressure was measured in situ with an accuracy of about 0.1 GPa using a standard ruby fluorescence scale.

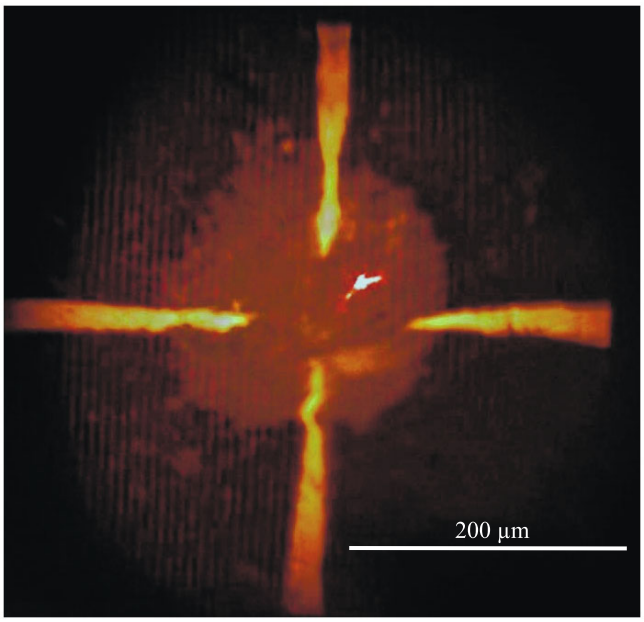

Fig. 1. (Color online) Micrograph of an $OsSe_2$ sample in a high-pressure cell with four platinum electrodes at a pressure of 38 GPa. The diamond culet size is 550 μm. A $RuSe_2$ sample was prepared and investigated at the same conditions.

EXPERIMENTAL RESULTS

Raman Spectroscopy

The evolution of Raman spectra of an $OsSe_2$ crystal under high-pressure is shown in Fig. 2a. The spectrum obtained at the lowest applied pressure of 0.7 GPa is similar to that reported in [17] for polycrystalline osmium diselenide at ambient pressure. The most intense peak (near to 219 cm^{-1}), corresponds to the A_g stretching mode of dumbbell-like Se–Se units. Besides it, there is a peak at about 230 cm^{-1} corresponding to the coupled stretching and librational mode T_g or to the E_g librational mode. Further Raman experiments on $OsSe_2$ single crystals in pure hydrostatic conditions are required for the reliable assignment of these modes. Unfortunately, only the Raman spectra of polycrystalline $OsSe_2$ sample are currently available [17].

Above 5–7 GPa, the pressure dependence of the shift of the Raman frequency modes $\Delta\nu(P)$ in $OsSe_2$ can be well approximated by a linear function (Fig. 3a). In the range of lower pressures, the experimental data points for the E_g mode do not follow the linear fit shown in Fig. 3a. Such nonlinear behavior may be related to the transition of $OsSe_2$ from single-crystal to powder form. The linear fit slopes of the experimental $\Delta\nu(P)$ curves for the $OsSe_2$ and $RuSe_2$ samples shown in Fig. 3 are presented in Table 1. A further increase in pressure results in a redistribution

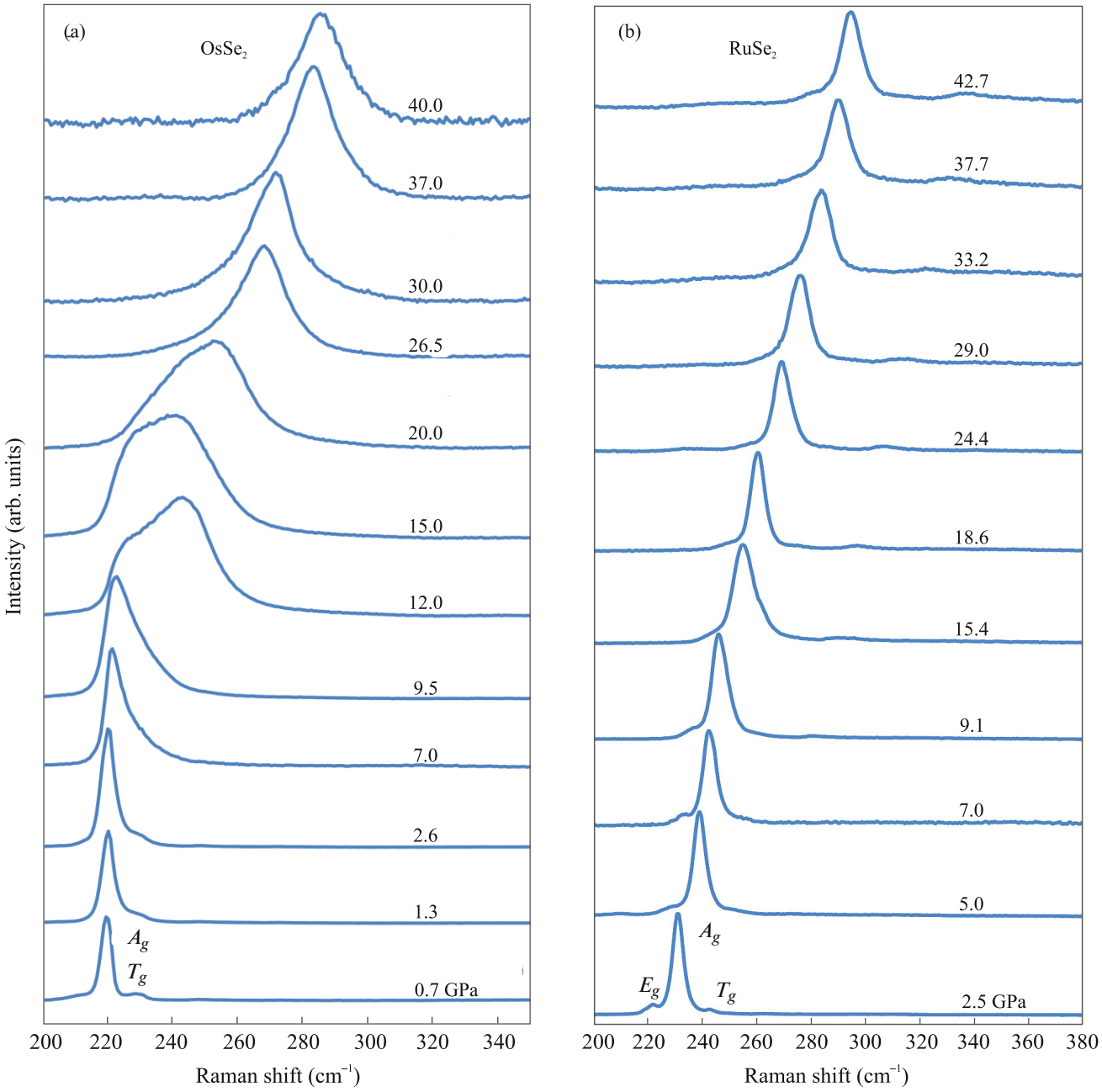

Fig. 2. (Color online) Raman spectra of (a) $OsSe_2$ and (b) $RuSe_2$ at various pressures.

of intensity between A_g and T_g modes, which occurs in the pressure range 9.5–26.5 GPa. Only the T_g mode is observed at higher applied pressures up to 40 GPa.

The evolution of Raman spectra of $RuSe_2$ under applied pressure (Fig. 2b) differs significantly from that for the $OsSe_2$ compound. At the lowest pressure of 2.5 GPa, three typical of pyrite-type structure peaks can be seen in $RuSe_2$: libration E_g, stretching A_g (most intensive) and coupled T_g. The Raman spectrum of the $RuSe_2$ single crystal at ambient conditions is well studied [17], so there are no problems with the determination of modes, as occurs in $OsSe_2$. In $RuSe_2$, there is no redistribution of mode intensity up to the highest applied pressure of 42.7 GPa, and the main A_g mode remains detectable over the entire pressure range. On the other hand, the intensities of both E_g and T_g modes vanish and are hardly detectable at pressures above 21.2 GPa (Fig. 2b). Their $\Delta\nu(P)$ curves can be approximated by linear dependences similar to $OsSe_2$ (Fig. 3b). The slopes for the T_g modes for both

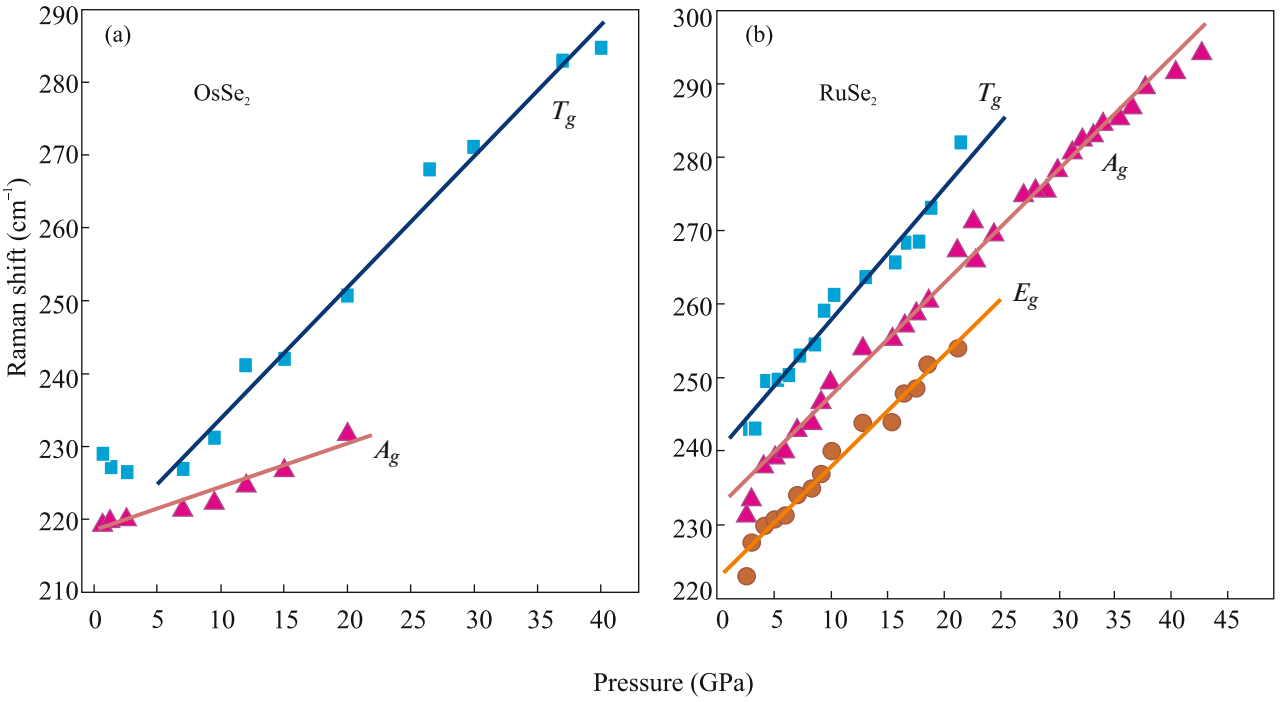

Fig. 3. (Color online) Positions of Raman modes versus the applied pressure for (a) $OsSe_2$ and (b) $RuSe_2$.

compounds are almost equal, as shown in Table 1, however, the slope for the A_g mode of $RuSe_2$ appears to be 2.6 times higher than that for $OsSe_2$.

Electrical Transport Measurements

The temperature dependences of the resistivity $\rho(T)$ of the $OsSe_2$ sample at constant high pressures are shown in Fig. 4a. It should be noted that at the lowest pressure of 0.7 GPa attained in our experiment, the form of the $\rho(T)$ curve is characteristic of semimetals. In the high temperature region, the resistivity decreases with decreasing temperature, while at low temperatures it increases, similar to the $\rho(T)$ behavior reported in [18] for $OsSe_2$ at ambient pressure. With increasing pressure from 2.6 GPa to about 40 GPa, a noticeable drop of the sample resistivity occurred over the entire temperature range, as shown in Fig. 5a. Under pressures above 15–20 GPa, we observed the metallic type of resistivity in the $OsSe_2$ sample at room temperature. The similar effects reported in [13, 14] were associated with a substantial overlapping of the conduction and valence bands.

Table 1. Linear fit slopes of the experimental Raman mode frequency obtained from the pressure dependences shown in Fig. 3 for $OsSe_2$ and $RuSe_2$

Sample	$OsSe_2$		$RuSe_2$		
$\frac{\partial\Delta\nu}{\partial P}, \frac{cm^{-1}}{GPa}$	A_g	T_g	E_g	A_g	T_g
	0.60	1.80	1.52	1.54	1.81

The sample resistivity remained almost unchanged with a further increase in pressure. We will consider this state to be metallic despite a slight increase in the sample resistivity observed at low temperatures (Fig. 5a). This effect is caused by the peculiarities of the Fermi surface of the material.

At pressures in the range of 20–40 GPa, the electrical resistance of the sample $OsSe_2$ drops in the temperature range 2–6 K (see the inset of Fig. 4a). This might be caused by a transition to the superconducting state. However, the sample resistance does not reach zero value, probably, due to the partial transition of the sample to the superconducting state. Nevertheless, an increase in pressure leads to an increase in the resistance drop value, which implies an increase in the fraction of the superconducting phase in the sample. This state is usually called filamentary superconductivity. The formation of this state may be due to the high sensitivity of the sample electronic properties to the nonhydrostatic environment of the sample in the DAC gasket hole [24]. A similar effect has recently been reported for ReS_2 [12].

We observed the transition to the superconducting state in $OsSe_2$ at all pressures above 20 GPa (inset of Fig. 4a). The pressure dependence of the critical transition temperature $T_c(P)$ is shown in Fig. 5a. The T_c value increases as the pressure increases to 40 GPa. Probably, this is just the ascending part of the dome-

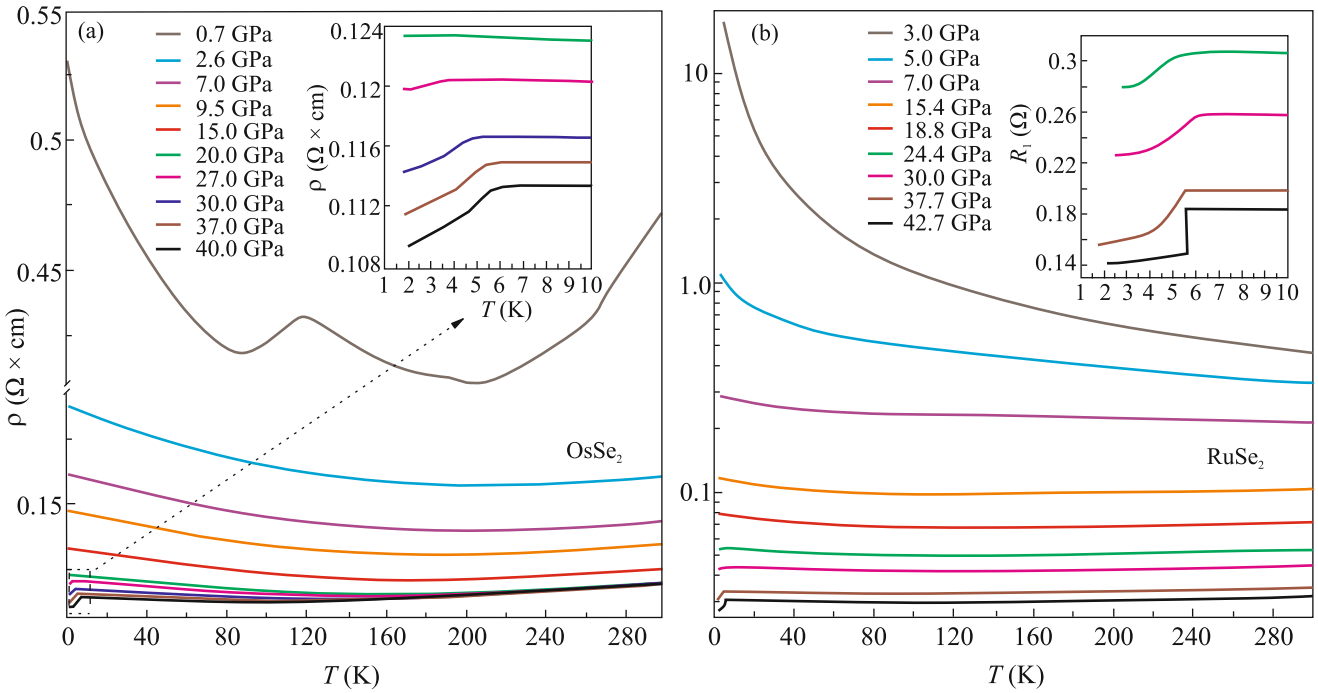

Fig. 4. (Color online) Temperature dependences of the resistivity in (a) $OsSe_2$ and (b) $RuSe_2$ measured in the pressure increase mode. The inset in panel (a) shows the resistivity of $OsSe_2$ at low temperatures. The inset in panel (b) shows the resistance from a single van der Pauw channel at low temperatures.

shaped curve. Thereby, an increase in the pressure to 40 GPa stabilizes the superconducting properties of $OsSe_2$.

The evolution of the $\rho(T)$ curves for the $RuSe_2$ sample (Fig. 4b) appears to be similar to that of the $OsSe_2$ compound. Being a semiconductor at ambient conditions, in the pressure range from 3 GPa to about 24 GPa, $RuSe_2$ behaves as a semiconductor and demonstrates a clear increase in resistivity in the low temperature range, as shown in Fig. 4b. The resistivity curves $\rho(T)$ are flattened with increasing pressure. The resistivity of the $RuSe_2$ sample at 300 K (Fig. 5b) also decreases with pressure, as it was observed in $OsSe_2$. Both the $\rho(T)$ curve flattening and resistivity drop at 300 K can be explained in terms of the collapse of the $RuSe_2$ band gap and the metallization of a sample similar to $OsSe_2$.

Under pressure, $RuSe_2$ also demonstrates a transition to the superconducting state (inset of Fig. 4b). Thus, a noticeable drop in resistivity at low temperatures is observed at pressures above 15 GPa and extends up to 43 GPa (inset of Fig. 4b). In contrast to $OsSe_2$, the $T_c(P)$ dependence for $RuSe_2$ does not have a dome-like shape. The T_c value in $RuSe_2$ reaches a plateau at about 5.5 K above 19 GPa and remains almost constant up to the highest applied pressure of 42.7 GPa (Fig. 5b).

DISCUSSION

In recent studies of superconductivity in TMD with a pyrite-type structure, the relationship between superconductivity and structural instability, which involves the destabilization of anionic dimers, has often been discussed. In $PdSe_2$, such destabilization is caused by the application of external pressure [13], and in $IrSe_2$ by Rh doping [15]. This kind of structural instability leads to a decrease in the frequency of the stretching A_g Se–Se mode due to an increase in the length of the Se–Se bond, as demonstrated by Raman spectroscopy.

However, for the PdS_2 and $NiSe_2$ dichalcogenides with a pyrite-type structure, it was shown that the destabilization of anionic dimers is not necessary for the occurrence of superconductivity, and such destabilization is not a sufficient condition for the formation of superconductivity [14]. Therefore, in PdS_2 there is no correlation between the softening of the S–S dumbbell bonds and the dependence $T_c(P)$. Meanwhile, despite the elongation of Se–Se bonds under pressure in $NiSe_2$, the sample remains a normal non-superconducting metal.

In our samples, weakening of the Se–Se chemical bonds in $OsSe_2$ and $RuSe_2$ under high pressure is not observed, which is confirmed by a constant increase in the frequency of the Ag mode with pressure in both compounds. Moreover, our Raman spectroscopy

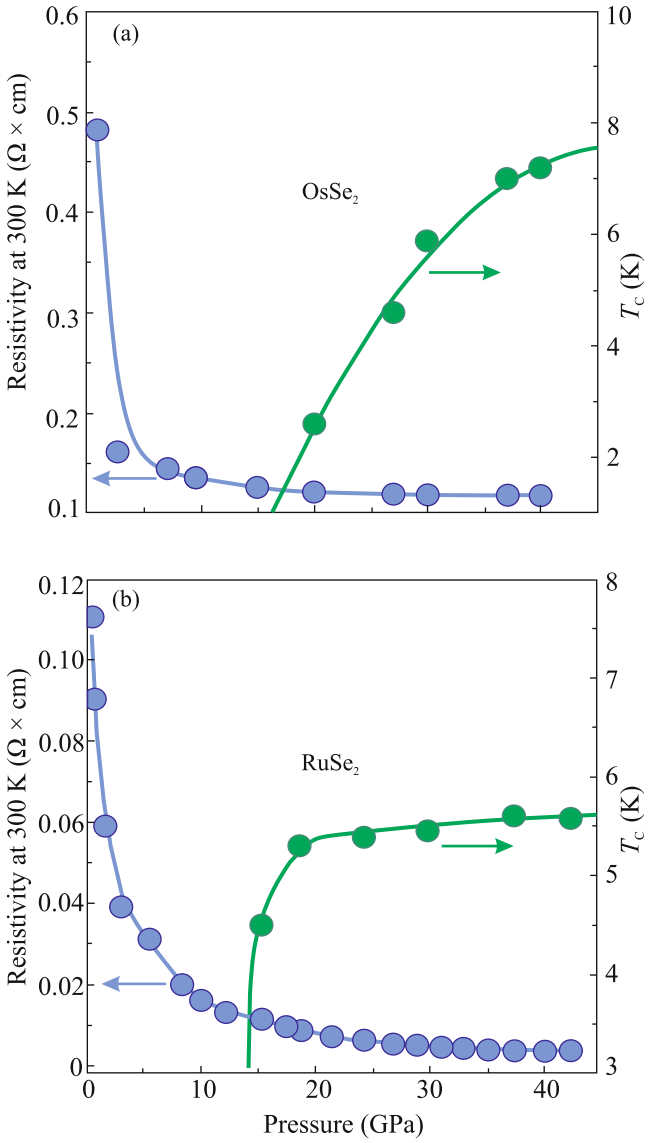

Fig. 5. (Color online) Pressure dependence of the room temperature resistivity and the onset temperature T_c of the superconducting transition for (a) $OsSe_2$ and (b) $RuSe_2$ compounds.

studies did not reveal any indication of structural phase transitions up to pressures of about 40 GPa. Thus, it can be assumed that the pyrite-type structure remains stable up to the highest pressures attained in the experiments. Thus, in contrast to $Ir_{1-x}Th_xSe_2$ or $PdSe_2$, the appearance of superconductivity in $OsSe_2$ and $RuSe_2$ is not due to a phase transition or instability of anionic dimmers. For both materials, a superconducting transition is observed at pressures above the transition to the metallic state, which is achieved during the slow evolution of semimetal into metal under pressure.

CONCLUSIONS

Single crystals $OsSe_2$ and $RuSe_2$ were investigated by Raman spectroscopy and electrical transport measurements at high pressures up to 40 GPa. Electrical resistivity measurements for both compounds revealed their metallization above 10–15 GPa. Transitions to the superconducting state were observed above ~15 GPa.

An increase in the critical temperature T_c with the pressure was found for both samples. $OsSe_2$ demonstrated the classic dome-shape behavior of $T_c(P)$ dependence, while for $RuSe_2$, the critical temperature T_c remains constant above 35 GPa. For both materials, no indications of a structural phase transition were found in our spectroscopic studies up to the highest pressures.

FUNDING

The work on the preparation of the high-pressure cells, loading of high-pressure cells, Raman and transport measurements at high pressures, analysis and processing of the results of these measurements, and preparation of the manuscript was supported by the Russian Science Foundation (project no. 17-72-20200). The sample characterization was supported by the Ministry of Science and Higher Education of the Russian Federation (state assignment for the FSRC Crystallography and Photonics, Russian Academy of Sciences).

REFERENCES

1. S. Manzeli, D. Ovchinnikov, D. Pasquier, O. V. Yazyev, and A. Kis, Nat. Rev. Mater. **2**, 17033 (2017).
2. Y.-H. Wang, K.-J. Huang, and X. Wu, Biosens. Bioelectron. **97**, 305 (2017).
3. M. Chhowalla, H. S. Shin, G. Eda, L.-J. Li, K. P. Loh, and H. Zhang, Nat. Chem. **5**, 263 (2013).
4. A. O. Baskakov, Y. L. Ogarkova, I. S. Lyubutin, S. S. Starchikov, V. Ksenofontov, S. I. Shylin, D. Kroitor', V. Tsurkan, S. A. Medvedev, and P. G. Naumov, JETP Lett. **109**, 536 (2019).
5. R. Z. Vitlina, L. I. Magarill, and A. V. Chaplik, JETP Lett. **110**, 540 (2019).
6. M. Luo, Y. H. Shen, and T. L. Yin, JETP Lett. **105**, 255 (2017).
7. H. Wang, H. Feng, and J. Li, Small **10**, 2165 (2014).
8. W. Choi, N. Choudhary, G. H. Han, J. Park, D. Akinwande, and Y. H. Lee, Mater. Today **20**, 116 (2017).
9. X. Fan, C.-H. Chang, W. T. Zheng, J.-L. Kuo, and D. J. Singh, J. Phys. Chem. C **119**, 10189 (2015).
10. Y. Qi, P. G. Naumov, M. N. Ali, et al., Nat. Commun. **7**, 11038 (2016).
11. B. Wang, Y. Liu, K. Ishigaki, K. Matsubayashi, J. Cheng, W. Lu, Y. Sun, and Y. Uwatoko, Phys. Rev. B **95**, 220501 (2017).

12. D. Zhou, Y. Zhou, C. Pu, X. Chen, P. Lu, X. Wang, C. An, Y. Zhou, F. Miao, C.-H. Ho, J. Sun, Z. Yang, and D. Xing, NPJ Quantum Mater. **2**, 19 (2017).
13. M. A. ElGhazali, P. G. Naumov, H. Mirhosseini, V. Süß, L. Müchler, W. Schnelle, C. Felser, and S. A. Medvedev, Phys. Rev. B **96**, 060509 (2017).
14. M. A. ElGhazali, P. G. Naumov, Q. Mu, V. Süß, A. O. Baskakov, C. Felser, and S. A. Medvedev, Phys. Rev. B **100**, 014507 (2019).
15. J. Guo, Y. Qi, S. Matsuishi, and H. Hosono, J. Am. Chem. Soc. **134**, 20001 (2012).
16. W. N. Stassen and R. D. Heyding, Can. J. Chem. **46**, 2159 (2006).
17. B. Müller and H. D. Lutz, Phys. Chem. Miner. **17**, 716 (1991).
18. Y. Yin, M. S. Fuhrer, and N. V. Medhekar, NPJ Quantum Mater. **4**, 1 (2019).
19. J. S. Sheu, Y. S. Shih, S. S. Lin, and Y. S. Huang, Mater. Res. Bull. **26**, 11 (1991).
20. K. Wang, A. Wang, A. Tomic, L. Wang, A. M. M. Abeykoon, E. Dooryhee, S. J. L. Billinge, and C. Petrovic, APL Mater. **3**, 041513 (2015).
21. X. Jiang, B. Mayers, Y. Wang, B. Cattle, and Y. Xia, Chem. Phys. Lett. **385**, 472 (2004).
22. W. Vogel, P. Kaghazchi, T. Jacob, and N. Alonso-Vante, J. Phys. Chem. C **111**, 3908 (2007).
23. X. Ding, F. Peng, J. Zhou, W. Gong, G. Slaven, K. P. Loh, C. T. Lim, and D. T. Leong, Nat. Commun. **10**, 1 (2019).
24. W. J. Duncan, O. P. Welzel, C. Harrison, X. F. Wang, X. H. Chen, F. M. Grosche, and P. G. Niklowitz, J. Phys.: Condens. Matter **22**, 052201 (2010).